NASA TECHNICAL NOTE

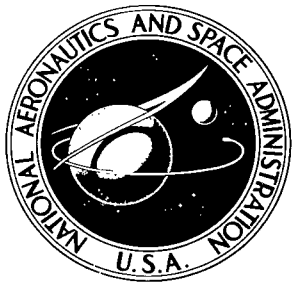

NASA TN D-6399

NASA TN D-6399

LEED AND AUGER ELECTRON SPECTROSCOPY STUDY OF OXYGEN ADSORPTION ON TUNGSTEN (110)

by Ronald G. Musket and John Ferrante

Lewis Research Center
Cleveland, Ohio 44135

NATIONAL AERONAUTICS AND SPACE ADMINISTRATION • WASHINGTON, D. C. • AUGUST 1971

1. Report No. NASA TN D-6399	2. Government Accession No.	3. Recipient's Catalog No.
4. Title and Subtitle LEED AND AUGER ELECTRON SPECTROSCOPY STUDY OF OXYGEN ADSORPTION ON TUNGSTEN (110)		5. Report Date August 1971 6. Performing Organization Code
7. Author(s) Ronald G. Musket and John Ferrante		8. Performing Organization Report No. E-6117
9. Performing Organization Name and Address Lewis Research Center National Aeronautics and Space Administration Cleveland, Ohio 44135		10. Work Unit No. 120-27 11. Contract or Grant No.
12. Sponsoring Agency Name and Address National Aeronautics and Space Administration Washington, D.C. 20546		13. Type of Report and Period Covered Technical Note 14. Sponsoring Agency Code
15. Supplementary Notes		

16. Abstract

Several aspects of oxygen adsorption on W(110) have been examined. Quantitative oxygen coverage as a function of oxygen exposure was determined in an Auger electron spectroscopy study. In particular coverages down to less than 0.02 monolayer of oxygen were detectable. The initial slope of the coverage against exposure curve provided a value of 0.23±0.05 for the initial sticking coefficient. Exposure dependence of the elastically back-scattered electrons and the electrons that suffered only a surface plasmon energy loss was found to be approximately the same as for the oxygen coverage. The total electron-impact cross section for the desorption of oxygen from an oxygen-saturated W(110) surface was determined to be $\sim 1.5 \times 10^{-20}$ cm^2 for 1365-eV electrons.

17. Key Words (Suggested by Author(s)) Auger spectroscopy Low energy electron diffraction Tungsten Oxygen adsorption	18. Distribution Statement Unclassified - unlimited

19. Security Classif. (of this report) Unclassified	20. Security Classif. (of this page) Unclassified	21. No. of Pages 35	22. Price* $3.00

*For sale by the National Technical Information Service, Springfield, Virginia 22151

LEED AND AUGER ELECTRON SPECTROSCOPY STUDY OF OXYGEN ADSORPTION ON TUNGSTEN (110)

by Ronald G. Musket and John Ferrante

Lewis Research Center

SUMMARY

Quantitative application of Auger electron spectroscopy has been demonstrated for the study of a gas on a surface. In particular, coverages down to less than 0.02 monolayer of oxygen were detectable on W(110). A conventional background-nulling technique permitted analysis of the oxygen Auger peak of the secondary electron energy distribution N(E); however, the constancy of the shape of the N(E) peak indicates that dN(E)/dE peaks would also be suitable for this study. With the area of the N(E) Auger peak taken as proportional to oxygen coverage, coverage as a function of exposure was found to saturate at exposures of 250 to 500 Langmuirs. If the saturated coverage corresponded to one monolayer of oxygen, then full development of the p(2×1) low energy electron diffraction (LEED) structure occurred for an exposure of 8.6 Langmuirs and a fractional coverage of 0.58, and the initial sticking coefficient was 0.23±0.05.

Previously reported characteristic energy loss values for clean W(110) were observed, and the losses of 13 and 23 eV were verified to result from surface- and bulk-plasmon excitations. The elastic peak, surface-plasmon peak, and oxygen coverage were found to have approximately the same dependence on exposure. This was explained in terms of scattering by the adsorbed oxygen.

Application of Auger electron spectroscopy to the determination of the total cross section for electron-impact desorption has been demonstrated for the desorption of oxygen from W(110). The total cross section was found to be $\sim 1.5 \times 10^{-20}$ square centimeter for 1365-eV electrons and an oxygen-saturated W(110) surface.

INTRODUCTION

Although oxygen (O) adsorption on tungsten (W) surfaces has been studied for many years, quantitative information on oxygen surface density is limited. However, such in-

formation is necessary for a thorough understanding of thermionic diode surfaces in the presence of oxygen. This report describes a room-temperature study which demonstrated the value of Auger electron spectroscopy (AES) and low energy electron diffraction (LEED) for such gas-surface systems. In particular, we determined the quantitative oxygen coverage (atoms on surface per unit area) as a function of oxygen exposure (molecules incident on surface per unit area) for W(110) surfaces. AES provided oxygen coverage data, and LEED provided complementary surface structure information. The value of AES for semiquantitative (refs. 1 and 2) and quantitative (ref. 3) concentration determinations had been demonstrated for deposition of metals on surfaces. Our study extends the quantitative application of AES to gases on surfaces. Future research should extend the studies to diode-like conditions.

Both AES and LEED results are determined by the properties of electrons scattered from surfaces. The secondary electron energy distribution N(E) is required in AES studies, while the scattering directions of diffracted electrons provide the LEED data. A brief discussion of N(E) and AES is presented in appendix A.

Previous AES studies employed the derivative dN(E)/dE of the secondary electron energy distribution N(E) with the peak-to-peak deflection at the Auger energy taken as proportional to the number of atoms present. This procedure assumes that the shape of the Auger peak, as resolved from N(E), remains unchanged throughout the experiment. When this assumption is valid, the peak-to-peak deflection of the dN(E)/dE curve is proportional to the amplitude and, hence, area of the resolved N(E) peak. A conventional background nulling technique permitted amplification and resolution of the N(E) peak. The area of this peak was taken as proportional to the oxygen coverage. The initial slope of the coverage against exposure data curve yielded the initial sticking coefficient.

Related studies include electronic desorption cross section for oxygen, variation in the elastic peak and characteristic loss peaks of N(E) with oxygen exposure, determination of LEED patterns and intensities as a function of exposure, and a study of tungsten Auger peaks under various surface conditions. Wherever possible, the results are compared with other studies.

EXPERIMENTAL CONSIDERATIONS

The basic apparatus was a Varian LEED system with low noise power supplies. The experimental arrangement displayed in figure 1 is similar to the one employed by Palmberg and Rhodin (ref. 2) except that the present arrangement includes a second retarding grid and provision for determination of both the secondary electron energy distribution N(E) and its derivative dN(E)/dE. The additional retarding grid substantially improved the energy resolution. LEED patterns were obtained by switching the fluorescent screen

connection from the bias battery to the fluorescence voltage. The values for the bias battery and signal resistor R_s were 600 volts and 1 megohm, respectively. Modulation of the retarding voltage was accomplished with a 4-volt peak-to-peak sinusoidal signal. All instruments were tuned to 325 hertz. A detailed discussion of the determination of N(E) and dN(E)/dE is presented in appendix B.

The input of the lock-in amplifier was operated in the A-B differential mode. N(E) curves ×1, ×4, and $\times 10^3$ in figure 2 were obtained without a signal at input B, although the zero of the lock-in amplifier output was shifted, or suppressed, for curve $\times 10^3$. Increasing the sensitivity above $\times 10^3$ was not possible because the tuned signal amplifier would have been overloaded. However, a conventional background-nulling technique permitted increasing the sensitivity by more than an order of magnitude. Curve $\times 10^4$ was obtained by applying a square-wave signal, from the ac offset, at input B. The amplitude and phase of the B signal were chosen to minimize, or null, the peak-to-peak output of the tuned signal amplifier with the retarding voltage V_r maintained at 525 volts. Since the chosen B signal nulled the input to the tuned signal amplifier, further increases in sensitivity were possible, in the region of the oxygen Auger peak, without overloading the amplifier. Under this condition the output of the lock-in amplifier was proportional to the difference between the nulled background level at V_r = 525 volts and the signal at input A. For the application of this technique the incident beam energy had to be chosen to yield a minimum in the N(E) background at the oxygen Auger peak. When a somewhat different beam energy was employed, the oxygen peak was buried in the steeply sloping background and resolution of the peak was impossible. Resolved peaks obtained by this technique should be valuable for quantitative atomic species determinations and for electronic structure analyses.

Final preparation of the tungsten single-crystal ribbon consisted of spark erosion planing to 1/4-millimeter thickness, a mechanical polishing, and electropolishing in a solution of 0.175 cubic centimeters (175 ml) water, 0.025 cubic centimeters (25 ml) hydrogen peroxide, and 4 grams of sodium hydroxide. Resultant ribbon dimensions were approximately 1/8 by 3 by 16 millimeters. Laue back-diffraction X-ray analysis indicated that the ribbon was within 1/2 degree of the (110) plane. The ribbon was spot-welded to tungsten support rods which permitted Ohmic heating of the ribbon. Heating the ribbon to between 2000 and 2600 K in oxygen pressures near 10^{-7} torr for 10 hours removed the carbon impurity. The ribbon was considered clean when, after prolonged heating in vacuum above 2500 K, the 270-eV carbon peak was absent from the Auger electron spectrum and the LEED pattern was characteristic of clean W(110). LEED patterns of carbon-contaminated and clean W(110) are shown in figure 3.

A 0.14-cubic-meter-per-second (140-liter/sec) Vacion pump and a water-cooled titanium sublimation pump maintained the background operating pressure at $\sim 6\times 10^{-10}$ torr. For studies of oxygen adsorption on W(110), oxygen was diffused through a silver

leak into the gas inlet manifold; then, with a manifold oxygen pressure near 1 torr, oxygen was admitted to the experimental chamber. For studies of oxygen adsorption on W(110), care must be taken to minimize the effect of carbon monoxide (refs. 4 and 5). Quadrupole mass spectrometry indicated that periodic argon instability treatments (appendix B) of the Vacion pump held the partial pressure ratio of oxygen and carbon monoxide (O_2/CO) above 100 for an oxygen pressure of 5×10^{-8} torr. This ratio has been shown to be sufficient for LEED studies on W(110) (ref. 5). All pressures were measured by a nude ion gage, but consideration was given to the error induced by the O^+ ion current resulting from electron impact desorption of oxygen adsorbed on the grid of the ion gage (refs. 6 and 7). The mass spectrometer was calibrated against the ion gage at oxygen pressures for which the O^+ current was not important ($>10^{-7}$ torr) (ref. 7); then the ion gage was compared to the mass spectrometer at lower oxygen pressures. This comparison was made by raising the pressure from below 10^{-9} torr to 5×10^{-8} torr oxygen; the mass spectrometer and the ion gage were found to agree within 5 percent. After tens of minutes, the ion gage was reading up to 10 percent higher than its initial oxygen value. Correction for this desorption effect was made in evaluating the pressure against time data recorded from the ion gage. The integral of the oxygen pressure over the time of adsorption yielded the oxygen exposure. We have expressed exposure in Langmuirs, where a Langmuir equals 10^{-6} torr second.

The procedure followed for all room temperature adsorptions was to (1) heat the ribbon above 2300 K for 1/2 minute, cool for 1/2 minute, and heat above 2300 K for 1/2 minute; (2) wait 2 minutes, then expose the ribbon to 5×10^{-8} torr oxygen for the desired time interval; and (3) record the N(E) curve at the oxygen Auger peak for 1365-eV incident electrons. Heating to an optical pyrometer temperature of 2300 K lowered the adsorbed oxygen concentration to below the detectable limit of the Auger electron spectrometer, which will be shown to detect less than 0.02 monolayer. From ribbon resistance against time data during an 8-minute cooling period following step (1), the temperature of the ribbon at the end of 2 minutes was estimated to be 330 K. Biasing the ribbon to 300 volts, both before and after the N(E) curve was recorded, permitted determination of the average incident electron current. The ~8-microampere electron beam bombarded the target throughout the adsorption procedure. For higher temperature adsorptions, steps (1) and (3) were followed but step (2) varied and is detailed with the results for each high temperature adsorption.

RESULTS

AES and LEED Studies

Typical N(E) curves for the energy region of the oxygen Auger peak are presented in figure 4. Lock-in amplifier sensitivities of 10 and 20 microvolts correspond to $\times 2 \cdot 10^4$ and $\times 10^4$, respectively, on the scale of figure 2. The given energy scale was determined from the retarding voltage and does not include a correction for the work function of the retarding grids. During the 2-minute waiting period following heating of the ribbon, some oxygen and carbon monoxide was adsorbed on the ribbon surface; however, this zero exposure coverage was periodically monitored and was corrected for in the results. A typical zero exposure (0-Langmuir) curve is presented in figure 4.

A curve resolver was employed to fit a combination of a straight line and Gaussian curves to the N(E) data curve at the oxygen Auger peak. The technique is shown in figure 5. Fitting with Lorentzian curves was also tried, but the fit was best with Gaussian curves. At this time no physical significance is attached to the Gaussian shape of the oxygen Auger peak. Electronic stripping of the fitted curve provided the resolved peak with the peak area taken as proportional to the oxygen coverage. The peak width at half maximum varied randomly from 6.2 to 6.8 eV; however, the shape of the resolved oxygen peak was considered to remain unchanged because the ± 0.3-eV variation was smaller than the resolution capability of the energy analyzer. Control measurements were made to ensure that the shape and width of 509-eV Auger peak were not characteristic of the analyzer. Application of a 1-volt peak-to-peak modulation signal to the analyzer gave a peak width of less than 3 eV for a 518-eV elastically scattered primary beam; this same modulation signal yielded a Gaussian oxygen Auger peak with a width of 6.4 eV. Thus, the shape and width of the 509-eV Auger peak were characteristic of room-temperature adsorption of oxygen on W(110). Since the shape and width of the N(E) peaks were unchanged, dN(E)/dE peaks should also be suitable for this study.

Each peak area was divided by the corresponding incident electron current yielding the normalized peak area $A(l)$ for an exposure of l Langmuirs. After subtracting the average $A(0)$ from each $A(l)$, the fractional oxygen coverage $\theta(l)$ was specified by assuming a monolayer coverage for the saturation area at large exposures ($l > 250$ Langmuirs). Fractional oxygen coverage as a function of exposure is presented in figure 6. Each data point resulted from a separate adsorption procedure, and the points represent adsorption at several different places on the crystal surface. A fractional coverage of 0.02 for the lowest exposure attempted gives a measure of the sensitivity of the technique. Oxygen coverage for low exposures is detailed in figure 7. The error bar represents the standard deviation for the average zero exposure coverage correction $\theta(0) = 0.05 \pm 0.02$.

Room temperature oxygen adsorption changed the p(1×1) LEED pattern of clean W(110) (fig 8(a)) to a p(2×1) pattern (fig. 8(b)) The development of the p(2×1) pattern was monitored by measuring the intensity of one of the additional half-order spots as a function of oxygen exposure. Figure 9 gives the results; the rate of development is much faster than the rate of decay and is consistent with the coverage given in figure 6. At 8.6 Langmuirs, the intensity was a maximum; this corresponds (fig. 6) to a fractional of 0.58 We observed the other LEED patterns (ref. 4) for room-temperature adsorption of oxygen on W(110). We observed a weak p(2×2) arrangement at ~160 Langmuirs and a p(1×1) pattern with a diffuse background at 250 to 500 Langmuirs.

The derivative of $\theta(l)$ with respect to l is proportional to the sticking coefficient (atoms on surface divided by atoms impinged) of oxygen on W(110). Taking the density of tungsten atoms in the (110) plane (1.42×10^{15} atoms/cm^2) as the density of one monolayer of adsorbate and taking 3.65×10^{14} molecules per square centimeter per second as the arrival rate for oxygen molecules at 10^{-6} torr results in an initial sticking coefficient S_o of 0.23 ± 0.05.

Following Germer and May (ref. 4), we heated the crystal in 5×10^{-8} torr of oxygen for 25 minutes (~106 Langmuirs) at 1250 K. The resulting LEED pattern is given in figure 10 From the area of the resultant oxygen Auger peak and our room-temperature results, we determined that the oxygen content of the surface was slightly more than one monolayer; however, if oxygen has diffused into the surface, significantly more oxygen may be present. Germer and May (ref 4) deduced this result from their LEED experiments.

Tungsten Auger peaks were determined for three different surface conditions in high resolution experiments where 2v = 1 volt peak to peak, $T_{RC}R_T = 0.5$ volt (see appendix B). For the conditions examined (fig. 11), we concluded that presence of oxygen on W(110) does not have a marked effect on the tungsten Auger transitions. Examination of these peaks for thickly oxidized tungsten would be very instructive because a shift of 4 eV has been reported for a heavily oxidized sample of polycrystalline tungsten (ref. 8).

Characteristic Energy Loss Studies

Electron energy distribution N(E) for 122-eV primary electrons on clean W(110) is presented in figure 12. Graphical integration shows that the elastically scattered electrons are only about 2 percent of the total secondary electrons. Characteristic energy losses (see appendix A) are quite apparent. In particular, the 13- and 23-eV losses have been identified (ref. 9) as surface- and bulk-plasmon losses, respectively Changes in the characteristic loss region of N(E) with room temperature oxygen adsorption on W(110) are shown in figure 13. These results were obtained with 2v = 0.5 volt peak to

peak and $T_{RC}R_T = 0.25$ volt (see appendix B). If the amplitude of the bulk-plasmon loss is assumed to be nearly independent of the exposure, the growth of the surface-plasmon loss with increasing exposure can be quantified. Normalization to the 354-Langmuir case and the incident electron current I and allowance for the increase in background yields the normalized change in surface-plasmon peak amplitude $\delta_{S,i}$ as a function of exposure l (fig. 14), where

$$\delta_{S,i} = \frac{(A_B - A_S)_0 - (A_B - A_S)_i}{(A_B - A_S)_0 - (A_B - A_S)_{354}} \cdot \frac{1}{I_i} \tag{1}$$

where $(A_B - A_S)_i$ is the difference between the bulk and surface peak amplitudes for an exposure of i Langmuirs and I_i is the electron current for that exposure. Fractional coverage as a function of exposure is shown for comparison purposes. In addition, the normalized change in the elastic peak amplitude $\delta_{E,i}$ is presented in figure 14 for the same set of data, with

$$\delta_{E,i} = \frac{A_{E,i} - A_{E,0}}{A_{E,354} - A_{E,0}} \frac{1}{I_i} \tag{2}$$

The width $W_{1/2}$ of the elastic peak was 1.2±0.05 eV.

The surface-plasmon amplitude A_S of a clean surface was also determined as a function of the angle of incidence α (i. e., the angle between the incoming electron beam and the normal to the surface). Relative to normal incidence the amplitude was 1.08 for $\alpha = 15^\circ$ and 1.20 for $\alpha = 30^\circ$. Although a 20 percent change was observed in A_S, the change in A_B was less than 1.4 percent.

Electron-Impact Desorption Studies

Electron-impact desorption of gas species adsorbed on metal surfaces can provide information about surface bonding. Since the excitation cross section for electron-impact desorption is comparable to that for ionization or excitation in free molecules ($\sim 10^{-16}$ cm^2), the small total desorption cross section ($\sim 10^{-19}$ to 10^{-21} cm^2) must result from rapid reformation of the bond by electron tunneling from the metal (refs. 10 and 11). Thus, the rate of tunneling and the desorption cross section should be dependent upon the adsorption state or bonding configuration.

In particular, the oxygen-tungsten system has received much attention (refs. 10 to 15). When an oxygen-covered tungsten surface is bombarded with electrons, O and O^+ are desorbed. This process has been studied by monitoring the work function (refs. 10

to 13) and the emitted ion current (refs. 14 and 15). Each technique permits determination of the total desorption cross section under certain conditions. Application of the work function technique is valid whenever the work function change is proportional to the coverage change. The ion current technique is applicable if the total and ionic cross sections have the same coverage dependence.

Our purpose was to make a more direct determination of the total cross section for electron-impact desorption of oxygen from W(110). In essence, the determination consists of recording the oxygen Auger peak as a function of bombardment time. After room temperature adsorption on clean W(110), the coverage (i.e., the area of the oxygen Auger peak) was determined as a function of bombardment time.

The rate of change of the oxygen coverage during desorption is given by

$$\frac{dn}{dt} = -n\varphi_e\sigma_T \tag{3}$$

where n is the oxygen surface density, t is the time after the first Auger result, φ_e is the flux of incident electrons, and σ_T is the total electron-impact desorption cross section. Integration of equation (3) gives

$$\frac{n}{n_o} = \exp\left(-\varphi_e\sigma_T t\right) \tag{4}$$

where n_o is the density given by the first Auger peak. Thus, a semilogarithmic plot of $\ln(n/n_o)$ against t should be linear with slope $-\varphi_e\sigma_T$ whenever σ_T is not a function of n.

Results for oxygen exposures of 245 and 363 Langmuirs are presented in figure 15 for bombardment by 1365-eV electrons. The electron beam was on during both exposures and each initial fractional coverage was within 7 percent of 0.93 (fig. 6). Desorption for long exposures was examined because desorption of oxygen from tungsten had been shown to be greatest for such exposures (ref. 15). The bombardments were done in a vacuum of $<10^{-9}$ torr with 7.8- and 7.2-microampere (245- and 363-Langmuir) electron beams over 3/4 millimeter diameter. Since the maximum error in the estimated beam area was a factor of two, the absolute value $\sigma_T \approx 1.5\times10^{-20}$ square centimeter could be in error by as much as a factor of two. The lines were fitted to the data by a least-squares technique.

The effect of electron-impact desorption on the $\theta(l)$ data after oxygen exposure has been considered. Figure 15 shows that the coverage decreases about 10 percent for a 10-minute bombardment time; but, since all of the $\theta(l)$ data were taken 8±2 minutes after the end of exposure, we assumed that the error induced in our relative peak areas was considerably less than 10 percent.

The effect of the electron beam during room-temperature exposure has also been considered. Exposures of 245 and 363 Langmuirs were obtained with the electron beam on during the exposure. The initial fractional coverages for both exposures were within 7 percent of 0.93. Such a result is not surprising. Consider exposures with the electron beam on; then rate of adsorption can be compared to the rate of desorption. The rate of change of coverage dn/dt during the exposure is given by

$$\frac{dn}{dt} = \nu S(n) - n\varphi_e\sigma_T(n) \tag{5}$$

where ν is the oxygen atom arrival rate (atoms/(cm^2)(sec)) and S(n) is the sticking coefficient. The desorption term $n\varphi_e\sigma_T(n)$ is most important for large n because both n and $\sigma_T(n)$ are large and S(n) is small. Under the experimental conditions employed ($P(O_2) = 5\times10^{-8}$ torr and $n_{max} = 1.42\times10^{15}$ atoms/cm^2), the minimum ratio of the adsorption to desorption terms was ~150 S(n). For sticking coefficients greater than 0.07, desorption would have less than a 10 percent effect on the coverage. Thus, the $\theta(l)$ results for large S(n) should be more meaningful than those for small S(n). Since the AES-determined coverage saturates at 250 to 500 Langmuirs, dn/dt = 0 and desorption balances adsorption giving 150 S(n) = 1; hence, $S(n) \approx 0.01$. Therefore, our saturation coverage corresponds to $S(n) \approx 0.01$, not S(n) = 0.

DISCUSSION

For the most part, comparison with other oxygen-tungsten adsorption studies will be limited to W(110) because the interaction of oxygen with tungsten is a function of crystallographic orientation. Discussions are grouped by the topics given in the RESULTS section.

AES and LEED Studies

In addition to the present AES study, the fractional oxygen coverage $\theta(l)$ has been determined by desorption mass spectrometry (ref. 16) and work function changes (refs. 5 and 17). For the mass spectrometric study, the desorption quantities were normalized by using the fact that the amount of desorbed atomic oxygen was independent of the adsorption temperature. The dependence of the work function on exposure yields the coverage as a function of exposure provided that work function change is proportional to coverage change. Fractional coverage can be determined by some normalization procedure. A

summary of these coverage results are presented in figure 16. The present AES study is the most direct determination of $\theta(\ell)$.

Comparison of figure 6 with the $\theta(\ell)$ curve of Tracy and Blakely (ref. 5) yields interesting results: (1) they assumed $\theta(\sim 6$ Langmuirs$) \approx 0.5$, and we found $\theta(6$ Langmuirs$) = 0.5$; (2) they found $\theta(1$ Langmuir$) \approx 0.25$, while we found $\theta(1$ Langmuir$) = 0.1$; and (3) they found $\theta \propto \ell^2$ for $0.1 < \ell < 1$ Langmuir, and we have data which seem to confirm their result. However, the uncertainty of our results in the $\ell < 1$ Langmuir region dictates that we consider the agreement to be limited.

The exposure reported to saturate the W(110) surface with oxygen varies considerably. Kohrt and Gomer (ref. 17) report the lowest exposure for saturation ℓ_{sat}, which was equivalent to an integrated molecular flux of ~7 Langmuirs at 300 K; however, their gas temperature was ~50 K. Carroll and Melmed (ref. 18) report $\ell_{sat} = 600$ Langmuirs which agrees well with the present result: $\ell_{sat} = 250$ to 500 Langmuirs.

Many evaluations of the initial sticking coefficient of oxygen on W(110) have been made; they are as follows: ~0.2 (ref. 19), ~0.1 (ref. 16), 0.22 (ref. 5), and 0.35 (ref. 17). These values are equal to the average sticking coefficient for $0 \leq \theta \leq 0.1$. The value ~0.2 includes a factor-of-two algebraic correction to the original report. Agreement of previous coefficients with the present result (0.23) is quite good.

Schematic representations of the LEED patterns for clean and oxygen-covered W(110) are shown in figure 17. LEED results are consistent with 0.5 monolayer of adsorbed oxygen for the completed p(2×1) structure, 0.75 monolayer for the p(2×2) structure, and monolayer for the oxygen-saturated structure (ref. 4). The present AES results indicate that the completed p(2×1) structure occurs for slightly more than 0.5 monolayer (i.e., $\theta = 0.58$); however, since the excess oxygen (<0.1 monolayer) may be preferentially adsorbed in regions which do not contribute to the LEED pattern (e.g., imperfections), the LEED and AES results are not inconsistent. The oxygen exposure required to complete the p(2×1) structure has been reported as 1.6 (ref. 4), 4.7 (ref. 18), and 5.8 Langmuirs (ref. 5); agreement with the present result of 8.6 Langmuirs is fair. The large variation in the reported exposures is probably due to experimental errors in determining the oxygen pressure.

The nature of the surface structure producing the LEED patterns from oxygen adsorption on W(110) is a major point of contention. Reconstruction of the tungsten surface has been proposed to account for the LEED patterns (refs. 4, 16, 18, 20, 21, and 22) but explanations of the patterns without invoking reconstruction have been presented (refs. 5, 23, and 24). Reconstruction has been defined as the spontaneous rearrangement of surface atoms of a crystal when foreign atoms are adsorbed upon it (ref. 21). Germer and May (ref. 4) propose that only one atomic layer is reconstructed, but they also present a more complex double-layer reconstruction model. Schematic representations of the two possibilities for formation of the p(2×1) pattern are given in figure 18. Single-layer

reconstruction requires $\theta = 1/2$ for the completed p(2×1) structure; double-layer reconstruction has an oxygen content in the final structure equivalent to $\theta = 1$. Our LEED and AES results, normalized by the $\theta(l)$ results of Ptushinskii and Chuikov (ref. 16), show that p(2×1) is fully developed for $\theta \approx 1/2$. Thus double-layer reconstruction appears very improbable.

However, our results are inconclusive regarding the existence of single-layer reconstruction. Since the tungsten atoms in a reconstructed surface would be in an environment very different from the clean surface case, the nature of the electronic bonding should be different in each case. Differences in electronic bonding should be manifested in changes of electron energy levels, and possibly, Auger transitions among the changed energy levels. We had this in mind when we examined the tungsten Auger peaks near 170 eV under various surface conditions (fig. 11). Since we found essentially no difference in the Auger peak structure for a clean surface and a reconstructed superstructure surface (ref. 4), we suggest the following three possible explanations:

(1) Reconstruction does not occur.

(2) Reconstruction occurs, but all levels involved in the Auger transitions shift by approximately the same amount. Hence, there is no significant difference in the tungsten Auger peaks.

(3) Reconstruction occurs, but tungsten atoms which do not participate in the reconstruction contribute strongly to the Auger peaks and mask the effect of those atoms taking part in the reconstruction.

This approach to the reconstruction question deserves further exploration.

Characteristic Energy Loss Studies

The present determination of the characteristic energy losses for clean tungsten (fig. 12) is compared with previous results in table I. Agreement is satisfactory. Furthermore, we verified a previous conclusion (ref. 9) that the losses at 13 and 23 eV were surface- and bulk-plasmon losses. This was accomplished by observing that the amplitude of the 13-eV loss changed with oxygen exposure (fig. 13) and angle of incidence while the 23-eV loss was essentially constant.

We believe our results showing that the elastic peak, and surface-plasmon peak, and the oxygen coverage vary with exposure in approximately the same way (fig. 14) can be explained in terms of scattering of the normal-incidence beam by the top atomic layer of the surface. In the plasmon case elastic scattering prior to entering the pure tungsten region would enhance the surface loss because surface plasmons can only be excited by electrons which have momentum components parallel to the surface; thus electrons scattered on entry could excite surface plasmons on entry, as well as on exit. The growth of the elastic peak with exposure probably results from elastic scattering by oxygen followed

by elastic backscatter by tungsten; the oxygen scattering reduces the backscattering angle and enhances the elastic peak. Our study quantifies the results of Tharp and Scheibner (ref. 9) who reported that the relative increase in the surface-plasmon peak was roughly proportional to coverage.

Electron-Impact Desorption Studies

Comparison of the present results ($\sigma_T = 1.5\times10^{-20}$ cm^2) with previous results for desorption of oxygen from tungsten is given in table II. Since σ_T varies with crystallographic orientation, comparison to the previous W(110) study seems most pertinent; however, even for this case the oxygen coverage and the electron energy are quite different from the present study. More detailed studies at lower coverages and lower electron energies are needed. Determination of the cross sections for higher energy electrons are also needed because such cross sections are important in other Auger electron spectroscopy studies. In the present study, the electrons desorbing the oxygen and the electrons initiating the Auger transitions had the same energy. However, desorption by low energy electrons could be monitored by periodically determining the coverage with a high energy beam which could initiate the Auger transitions.

CONCLUSIONS

Quantitative application of Auger electron spectroscopy has been demonstrated for the study of a gas on a surface. In particular, coverages down to less than 0.02 monolayer of oxygen were detectable on W(110). A conventional background-nulling technique permitted analysis of the N(E) oxygen Auger peak where N(E) is the secondary electron energy distribution; however, the constancy of the shape of the N(E) peak indicates that dN(E)/dE peaks would also be suitable for this study. With the area of the N(E) Auger peak taken as proportional to oxygen coverage, coverage as a function of exposure was found to saturate at exposures of 250 to 500 Langmuirs. If the saturated coverage corresponded to one monolayer of oxygen, then full development of the p(2×1) low energy electron diffraction (LEED) structure occurred for an exposure of 8.6 Langmuirs and a fractional coverage of 0.58, and the initial sticking coefficient was 0.23±0.05.

Tharp and Scheibner's characteristic energy loss values for clean W(110) were observed, and the losses of 13 and 23 eV were verified to result from surface- and bulk-plasmon excitations. The elastic peak, surface-plasmon peak, and oxygen coverage were found to have approximately the same dependence on exposure. This was explained in terms of scattering by the adsorbed oxygen.

Application of Auger electron spectroscopy (AES) to the determination of the total cross section for electron-impact desorption has been demonstrated for the desorption of oxygen from W(110). The total cross section was found to be $\sim 1.5 \times 10^{-20}$ square centimeter for 1365-eV electrons and an oxygen-saturated W(110) surface.

The variety of results obtained in this series of studies is indicative of the applicability and versatility of LEED-AES equipment.

Lewis Research Center,
National Aeronautics and Space Administration,
Cleveland, Ohio, April 6, 1971,
120-27.

APPENDIX A

SECONDARY ELECTRON ENERGY DISTRIBUTION AND AUGER ELECTRON SPECTROSCOPY

When a monoenergetic beam of electrons strikes a surface, secondary electrons are emitted from the surface. If the incident beam has an energy E_0, the secondary electron energy distribution N(E) will have a shape similar to that presented in figure 19. Energy region I contains the elastically scattered electrons. If the elastically scattered electrons of region I are coherent, then they contribute to the LEED pattern. The incoherent electrons from region I provide the diffuse background of the diffraction pattern. The electrons which have suffered discrete energy losses are found in region II. Most Auger electrons are found in region III. The large peak in region IV contains the true secondaries, that is, the diffuse electrons.

The discrete loss peaks of region II contain primary electrons which have lost amounts of energy characteristic of the target material (ref. 25). The magnitude of the characteristic energy loss is independent of the incident beam energy. Excitation losses for electronic interband transitions and plasma oscillations adequately explain the characteristic losses. Viatskin (refs. 26 and 27) has shown that the average energy required for an interband transition is approximately

$$\Delta E_n = \frac{\hbar^2}{2m} \vec{n}^2 \tag{A1}$$

where m is the electron effective mass and $\vec{n}/2\pi$ is a reciprocal lattice vector. Plasma losses result from collective excitations (plasmons) of electrons in the solid. The excitation energy for such losses may be written as (ref. 28)

$$\Delta E_p \approx \hbar\omega_p \tag{A2}$$

where ω_p is the plasma frequency and

$$\omega_p^2 = \frac{4\pi\rho e^2}{m} \tag{A3}$$

where ρ equals the free electron density. If the number of free electrons per atom is assumed to equal the maximum number of valence electrons per atom, then good agreement is usually found between observed and calculated plasma losses for metals. The presence of a clean, planar solid-vacuum interface has been shown (ref. 29) to permit a surface-plasmon loss

$$\Delta E_S = \frac{\hbar\omega_p}{\sqrt{2}} \tag{A4}$$

If there is a surface layer with dielectric constant ϵ_o, then the surface-plasmon loss becomes (ref. 30)

$$\Delta E_S = \frac{\hbar\omega_p}{\sqrt{1 + \epsilon_o}} \tag{A5}$$

Auger electron transitions can be described with reference to figure 20. If the inner level, $E_I - \varphi_c$ of an atom is ionized, an electron from an outer level, $\epsilon + \delta$, will fill the vacancy. Then atomic de-excitation can occur by X-ray emission or by Auger electron emission. For materials with atomic number $Z \leq 32$ Auger electron emission predominates following K shell ionizations. The kinetic energy of the Auger electron for the transition shown in figure 20 is $E_A = E_I - 2(\varphi_c + \epsilon)$. Since φ may vary from 0 to $E_B - \varphi_c$, the Auger electrons from this transition will have an energy spread of $E_B - \varphi_c$. The Auger peak for carbon on tungsten is shown in figure 19. Although the transition of figure 20 involves an inner level and the conduction band, the transition may be between an inner level and an outer level for high atomic number species. The measured electron energy E_M is related to the Auger energy by

$$E_A = E_M + \varphi_G \tag{A6}$$

where φ_G is the work function of the analyzer.

APPENDIX B

EXPERIMENTAL DETAILS

Determination of N(E) and dN(E)/dE

A retarding-potential modulation technique was employed to obtain N(E) and dN(E)/dE. A small sinusoidal signal $v \sin \omega t$ was superimposed on the retarding potential which was applied on the two center hemispherically shaped grids (fig. 1). When only a dc retarding potential V is applied, the electron current I reaching the fluorescent screen will decrease as the retarding potential is increased (fig. 21). If $v \sin \omega t$ is applied for a fixed value V_o of the retarding potential, then the electron current will contain an ac component with an amplitude proportional to $dI/dV|_{V_o}$ (fig. 21). Since V is proportional to the electron energy E and ϵ is proportional to the amplitude v of the applied ac signal, the electron intensity can be expanded in a Taylor series about the energy E_o as indicated in figure 21. With the identifications of $E - E_o = \epsilon \sin \omega t$, $N(E) = dI/dE$, and $dN/dE = d^2I/dE^2$, I(E) is given by the equation in figure 21. The amplitude $A_1(E_o)$ of the fundamental component is given by

$$A_1(E_o) = \epsilon N(E_o) + \frac{\epsilon^3}{8} \left. \frac{d^2N}{dE^2} \right|_{E_o} + \cdots$$

which is nearly proportional to $N(E_o)$ if ϵ (i.e., v) is sufficiently small. The increase of the error in A_1 with increasing modulation amplitude v is discussed by Taylor (ref. 31). For an Auger peak with a Gaussian distribution, that is,

$$N(E) \propto e^{-(E-E_A)^2/2\sigma^2}$$

he shows that the maximum error in A_1 is ~6 percent when $v/\sigma \approx 0.7$. Since the full width at half height (FWHH) equals $2.36\,\sigma$, the error in A_1 is ~6 percent when $2v/\text{FWHH} \approx 0.6$. Analogously, the amplitude $A_2(E_o)$ of the second harmonic is nearly proportional to $dN/dE|_{E_o}$. Taylor found the error in A_2 to be ~6 percent when $v/\sigma \approx 0.6$. By varying E_o, both N(E) and dN(E) can be obtained. Experimentally, the lock-in amplifier permits determination of A_1 and A_2.

Choice of the peak-to-peak modulation amplitude 2v was made by compromise between the N(E) peak width and the amplitude of the $\sin \omega t$ component A_1. From the preceding, we know that $A_1 \propto v$; variation of the peak width with v was determined

experimentally. The result for a 518-eV elastically scattered beam is presented in figure 22. Contributions to the minimum peak width (~2.8 eV) include effects of electron gun energy dispersion, small inelastic collisions, design resolution of the four grid systems (FWHH/E $\approx$ 0.5 percent or 2.5 eV), and the product of the lock-in amplifier time constant T_{RC} and the total sweep rate R_T ($T_{RC}R_T$ = 0.135 V).

Most of the minimum width of figure 22 results from the resolution limit of the retarding grid system; however, for increased sensitivity with low noise it is desirable to increase the time constant T_{RC}. When T_{RC} is increased, the retarding potential sweep rate R_T must be decreased if the proper peak shape and amplitude is desired. Ideally, the product of $T_{RC}R_T$ should be zero; however, practical consideration require a nonzero value for $T_{RC}R_T$. With this in mind, we have investigated the experimental dependence of the peak height and width on the product $T_{RC}R_T$ for our instrumentation; the results are shown in figure 23 for the case of 518-eV electrons. Since the modulation voltage was 2 volts peak to peak, the minimum peak width was $W_{1/2} \approx 3$ eV (fig. 22). For $T_{RC}R_T < 0.2$ volt, there is negligible effect (<3 percent) on the peak height and width. For $T_{RC}R_T$ = 1.0 volt, the peak height was 71 percent of the "true" ($T_{RC}R_T \leq 0.01$ V) height and the width was increased by 38 percent; however, such a $T_{RC}R_T$ product would be suitable for a study of relative heights and widths of a given peak under various surface conditions. Furthermore, for the wider Auger peaks (e.g., $W_{1/2} \approx 6$ eV) the errors in the height and width should be considerably smaller.

The present study of the 509-eV oxygen Auger peak was accomplished with a modulation voltage of 4 volts peak to peak and a $T_{RC}R_T$ product of 1.0 volt. Peak width was found to be 6.5±3 eV for both 4- and 1-volt peak-to-peak modulation signals. The $T_{RC}R_T$ influence on the peak height could not be determined because the noise present at the high sensitivity required for Auger analysis precluded $T_{RC}R_T$ products below 1.0 volt. Since 2v/FWHH = 4/6.5 = 0.62, the error in A_1 was ~6 percent, aside from $T_{RC}R_T$ considerations.

Argon Instability Treatments

Periodic argon instability treatments of the Vacion pump were necessary to hold the O_2/CO ratio above 100 for an oxygen pressure of 5×10^{-8} torr. Although an operating vacuum of 5×10^{-10} torr was readily achieved following a bakeout, admission of high-purity oxygen to 5×10^{-8} torr resulted in $O_2/CO \approx 30$. The tendency of the pump to liberate previously pumped gases can be reduced by an argon treatment (ref. 32). The method employs the well-known argon instability characteristics of some sputter ion pumps. The method consisted of admitting argon to 2×10^{-6} torr to initiate instability cycles (period of ~2 min) with a maximum pressure of 5×10^{-5} torr; after several cycles,

argon flow was abruptly stopped at the start of a cycle (i.e., when the pressure began to rise). After the rapid pumpdown, oxygen was admitted to 5×10^{-8} torr with $O_2/CO > 100$. During the instability, deposition of considerable titanium gettering material probably buries the previously pumped gases under a thick layer of titanium. This procedure may not apply to super Vacion pumps, because of sputter cathode design.

REFERENCES

1. Weber, R. E.; and Peria, W. T.: Use of LEED Apparatus for the Detection and Identification of Surface Contaminants. J. Appl. Phys., vol. 38, no. 11, Oct. 1967, pp. 4355-4358.

2. Palmberg, P. W.; and Rhodin, T. N.: Auger Electron Spectroscopy of fcc Metal Surfaces. J. Appl. Phys., vol. 39, no. 5, Apr. 1968, pp. 2425-2432.

3. Weber, R. E.; and Johnson, A. L.: Determination of Surface Structures Using LEED and Energy Analysis of Scattered Electrons. J. Appl. Phys., vol. 40, no. 1, Jan. 1969, pp. 314-318.

4. Germer, L. H.; and May, J. W.: Diffraction Study of Oxygen Adsorption on a (110) Tungsten Face. Surface Sci., vol. 4, 1966, pp. 452-470.

5. Tracy, J. C.; and Blakely, J. M.: The Kinetics of Oxygen Adsorption on the (112) and (110) Planes of Tungsten. Surface Sci., vol. 15, 1969, pp. 257-276.

6. Redhead, P. A.: The Effects of Adsorbed Oxygen on Measurements with Ionization Gauges. Vacuum, vol. 13, no. 7, 1963, pp. 253-258.

7. Singleton, J. H.: Interaction of Oxygen with Hot Tungsten. J. Chem. Phys., vol. 45, no. 8, Oct. 15, 1966, pp. 2819-2826.

8. Haas, T. W.; Grant, J. T.; and Dooley, G. J., III: Some Problems in the Analysis of Auger Electron Spectra. J. Vac. Sci. Tech., vol. 7, no. 1, Jan.-Feb. 1970, pp. 43-45.

9. Tharp, L. N.; and Scheibner, E. J.: Energy Spectra of Inelastically Scattered Electrons and LEED Studies of Tungsten. J. Appl. Phys., vol. 38, no. 8, July 1967, pp. 3320-3330.

10. Menzel, Dietrich; and Gomer, Robert: Desorption from Surfaces by Slow-Electron Impact. J. Chem. Phys., vol. 40, no. 4, Feb. 15, 1964, pp. 1164-1165.

11. Menzel, Dietrich; and Gomer, Robert: Desorption from Metals by Low-Energy Electrons. J. Chem. Phys., vol. 41, no. 11, Dec. 1, 1964, pp. 3311-3328.

12. Zingerman, Ya. P.; Ishchuk, V. A.: Investigation of the Process of Sorption of Oxygen on (100) and (110) Faces of a Tungsten Single Crystal Using the Electron-Stimulated Desorption Effect. Soviet Phys.-Solid State, vol. 9, no. 3, Sept, 1967, pp. 623-629.

13. Zingerman, Ya. P.; and Ishchuk, V. A.: Double-Layer Adsorption of Oxygen on the (100) Face of a Tungsten Crystal at Room Temperature. Soviet Phys.-Solid State, vol. 10, no. 12, June 1969, pp. 2960-2961.

14. Yates, J. T., Jr.; Madey, T. E.; and Payn, J. K.: Desorption by Electron Impact: Carbon Monoxide, Nitric Oxide and Oxygen on Tungsten. Nuovo Cimento Suppl., vol. 5, no. 2, 1967, pp. 558-581.

15. Madey, Theodore E.; and Yates, John T., Jr.: Desorption by Electron Impact: Oxygen adsorbed on Tungsten. Surface Sci., vol. 11, 1968, pp. 327-351.

16. Ptushinskii, Yu. G.; and Chuikov, B. A.: Mass-Spectrometric Investigation of the Interaction of Oxygen with (110) and (100) Faces of a Tungsten Single Crystal. Soviet Phys.-Solid State, vol. 10, no. 3, Sept. 1968, pp. 565-570.

17. Kohrt, Carl; and Gomer, Robert: Adsorption of Oxygen on the (110) Plane of Tungsten. J. Chem. Phys., vol. 52, no. 6, Mar. 15, 1970, pp. 3283-3294.

18. Carroll, J. J.; and Melmed, A. J.: Ellipsometry - LEED Study of the Adsorption of Oxygen on (011) Tungsten. Surface Sci., vol. 16, 1969, pp. 251-264.

19. Zingerman, Ya. P.; and Ishchuk, V. A.: Adsorption of Oxygen on the (110) Face of a Tungsten Single Crystal. Soviet Phys.-Solid State, vol. 8, no. 3, Sept. 1966, pp. 728-733.

20. Vas'ko, N. P.; Ptushinskii, Yu. G.; and Chuikov, B. A.: On the State of Oxygen Adsorbed on the Surface of Tungsten and Molybdenum Single Crystals. Surface Sci., vol. 14, 1969, pp. 448-456.

21. Germer, L. H.: The Uncertainty Regarding Reconstructed Surfaces. Surface Sci., vol. 5, 1966, pp. 147-151.

22. May, John W.: A Mechanism for Surface Reconstruction at Room Temperature. Surface Sci., vol. 18, 1969, pp. 431-436.

23. Bauer, E.: Comments on "The Uncertainty Regarding Reconstructed Surfaces" by L. H. Germer. Surface Sci., vol. 5, 1966, pp. 152-154.

24. Ducros, P.: Sur la Possibilité D'invoquer L'effet Jahn-Teller pour Interpréter les Déformations Permanentes Détectées par la Diffraction des Électrons Lents sur les Faces Denses du Silicium et du Germanium. Surface Sci., vol. 10, 1968, pp. 295-298.

25. Raether, H.: Solid State Excitations by Electrons (Plasma Oscillations and Single Electron Transitions). Springer Tracts in Modern Physics. Vol. 38. Hoehler, G., ed., Springer-Verlag, 1965, pp. 85-157.

26. Viatskin, A. Ia.: The Theory of Inelastic Scattering of Electrons in Metals. I. Soviet Phys.-Tech. Phys., vol. 3, no. 10, Oct. 1958, pp. 2038-2047.

27. Viatskin, A. Ia.: The Theory of Inelastic Scattering of Electrons in Metals. II. Soviet Phys.-Tech. Phys., vol. 3, no. 11, Nov. 1958, pp. 2252-2264.

28. Klemperer, O.; and Shepherd, J. P. G.: Characteristic Energy Losses of Electrons in Solids. Adv. Phys., vol. 12, no. 48, Oct. 1963, pp. 355-390.

29. Ritchie, R. H.: Plasma Losses by Fast Electrons in Thin Films. Phys. Rev., vol. 106, no. 5, June 1, 1957, pp. 874-881.

30. Stern, E. A.; and Ferrell, R. A.: Surface Plasma Oscillations of a Degenerate Electron Gas. Phys. Rev., vol. 120, no. 1, Oct. 1, 1960, pp. 130-136.

31. Taylor, N. J.: Resolution and Sensitivity Considerations of an Auger Electron Spectrometer Based on Display LEED Optics. Rev. Sci. Instr., vol. 40, no. 6, June 1969, pp. 792-804.

32. Chang, Chuan C.: Low Energy Electron Diffraction Studies, Adsorption of O_2, CO and N_2 on the Tungsten (112) Face. Ph.D. Thesis, Cornell Univ., 1967.

33. Harrower, G. A.: Auger Electron Emission in the Energy Spectra of Secondary Electrons from Mo and W. Phys. Rev., vol. 102, no. 2, Apr. 15, 1956, pp. 340-347.

34. Powell, C. J.; Robins, J. L.; and Swan, J. B.: Effects of Contamination on the Characteristic Loss Spectrum of Tungsten. Phys. Rev., vol. 110, no. 3, May 1, 1958, pp. 657-660.

TABLE I. - CALCULATED AND OBSERVED CHARACTERISTIC ENERGY LOSSES FOR TUNGSTEN

(a) Observed

Characteristic energy losses, eV					Sample	Source
13	23	35	43	53	Clean W(110)	Present results (see fig. 12)
12.5	23.5	35	43	53.5	Clean W(110)	Tharp and Scheibner (ref. 9)
14.8	26.8	--	46.4	58.0	Polycrystalline ribbon	Harrower (ref. 33)
10.6	24.3	--	43.3	52.8	Polycrystalline wire	Powell, Robbins, and Swan (ref. 34)

(b) Calculated

Characteristic energy losses, eV					Mechanism	Source
16.2	22.8	--	--	--	Plasmon excitation	Eqs. (A3) and (A4)
15	----	30	45	60	Interband transitions	Viatskin (refs. 26 and 27)

CS-58869

TABLE II. - ELECTRON-IMPACT DESORPTION CROSS SECTIONS

Tungsten surface	Electron energy, E, eV	Oxygen coverage	Cross section, cm^2	Source
W(110) ribbon	1365	High	$\sim 15\times10^{-21}$	Present results
W(110) disk	300	Low	$\sim 9\times10^{-21}$	Ref. 12
W(100 disk	300	Low	$\sim 60\times10^{-21}$	Ref. 12
Field emission tip	15 to 200	Low to high	$<2\times10^{-21}$ to 450×10^{-21}	Refs. 10 and 11
Polycrystalline ribbon	100	High	700×10^{-21}	Refs. 14 and 15

CS-58870

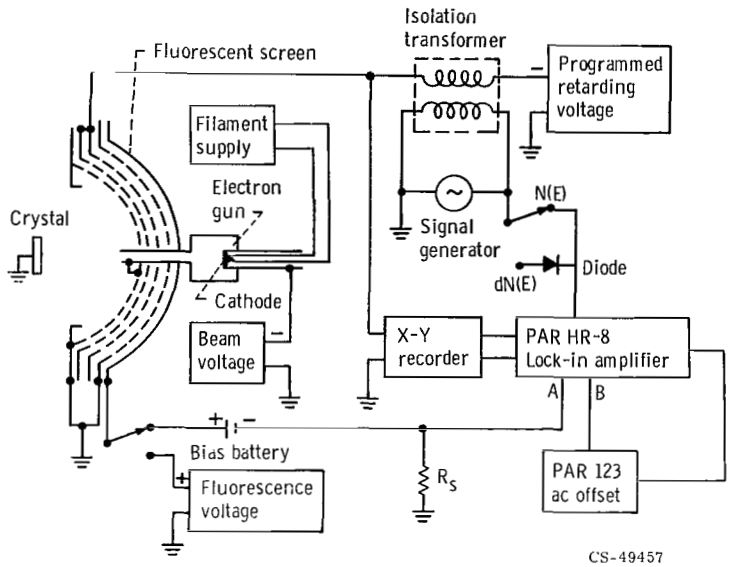

Figure 1. - Schematic of experimental arrangement.

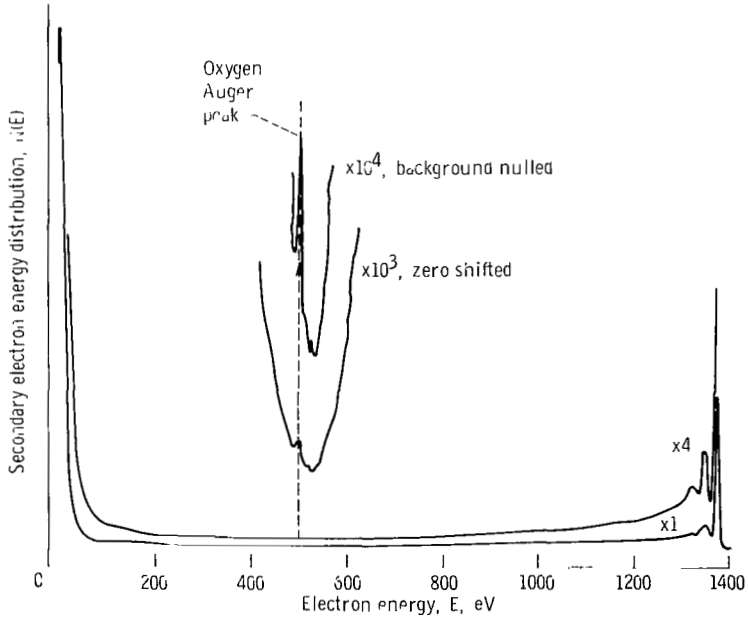

Figure 2. - Secondary electron energy distribution for 1365-eV electrons incident on W(110) exposed to 7.5 Langmuirs of oxygen.

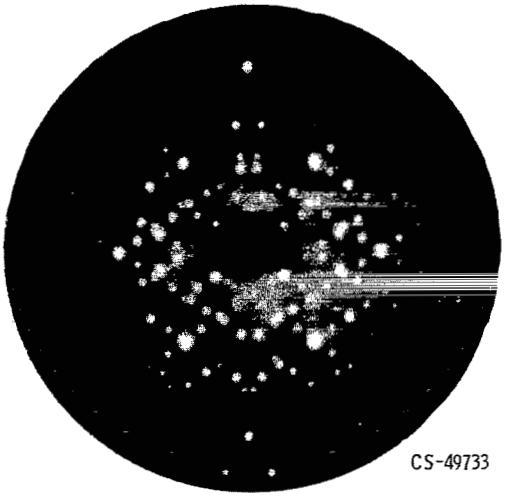

(a) Carbon-contaminated W(110).

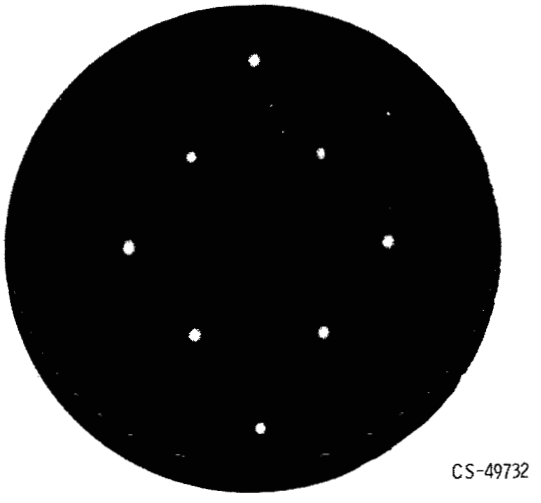

(b) Clean W(110).

Figure 3. - LEED patterns at 206 eV of carbon-contaminated W(110) and clean W(110).

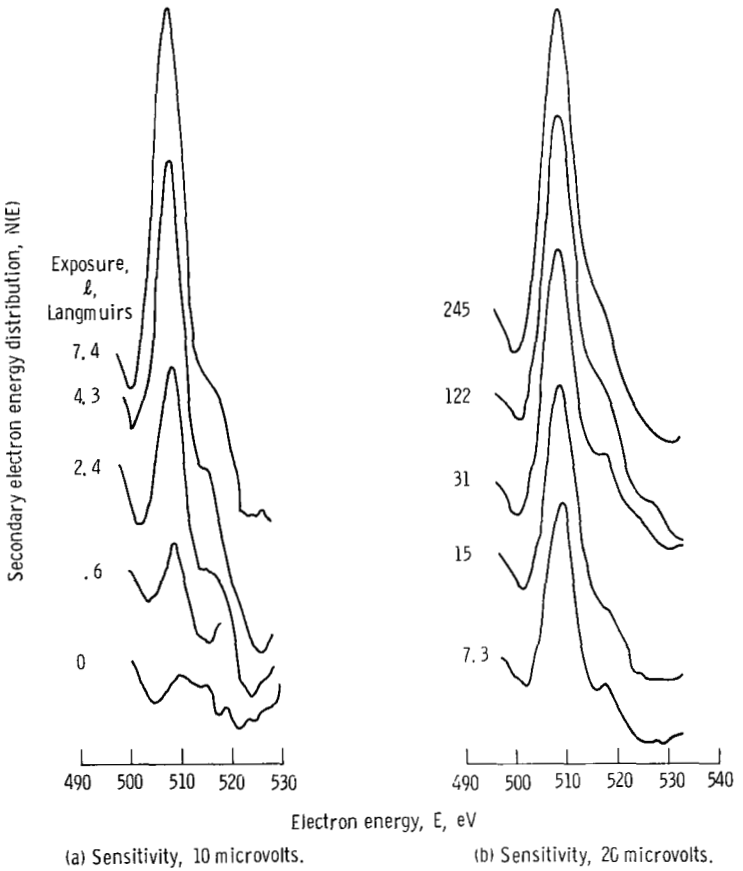

CS-51058

(a) Sensitivity, 10 microvolts. (b) Sensitivity, 20 microvolts.

Figure 4. - Oxygen Auger peaks for representative oxygen exposures.

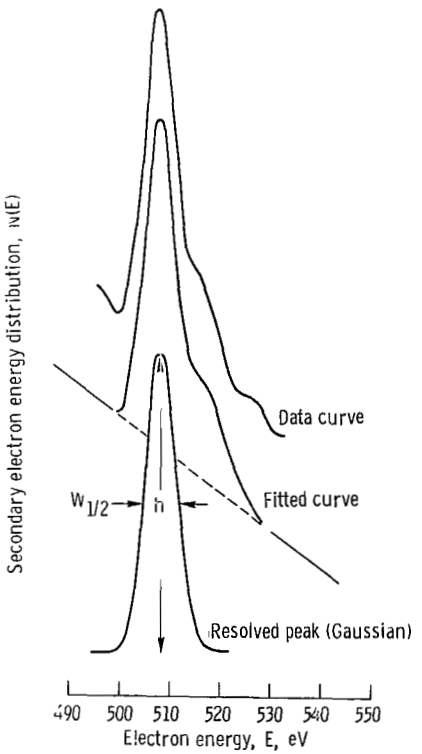

CS-51057

Figure 5. - Auger peak resolving technique. Area $\propto hW_{1/2}$.

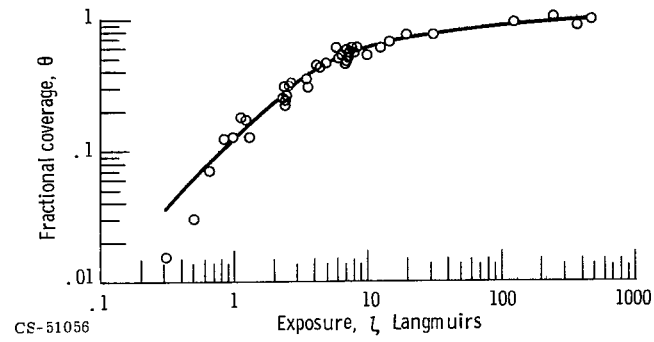

Figure 6. - Oxygen coverage on W(110) as a function of oxygen exposure.

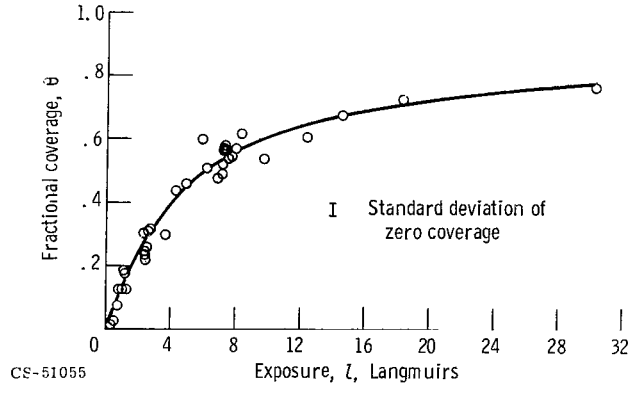

Figure 7. - Oxygen coverage on W(110) for low oxygen exposures.

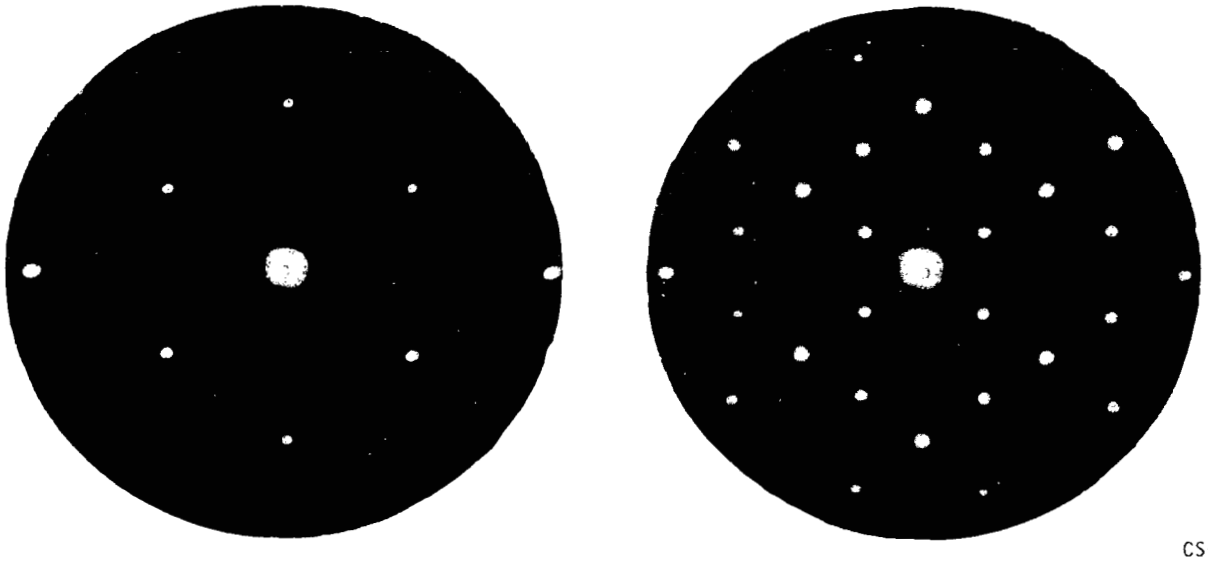

CS-50728

(a) Clean W(110).

(b) p(2x1) oxygen structure on W(110).

Figure 8. - LEED patterns at 119 eV of clean W(110) and p(2x1) oxygen structure on W(110).

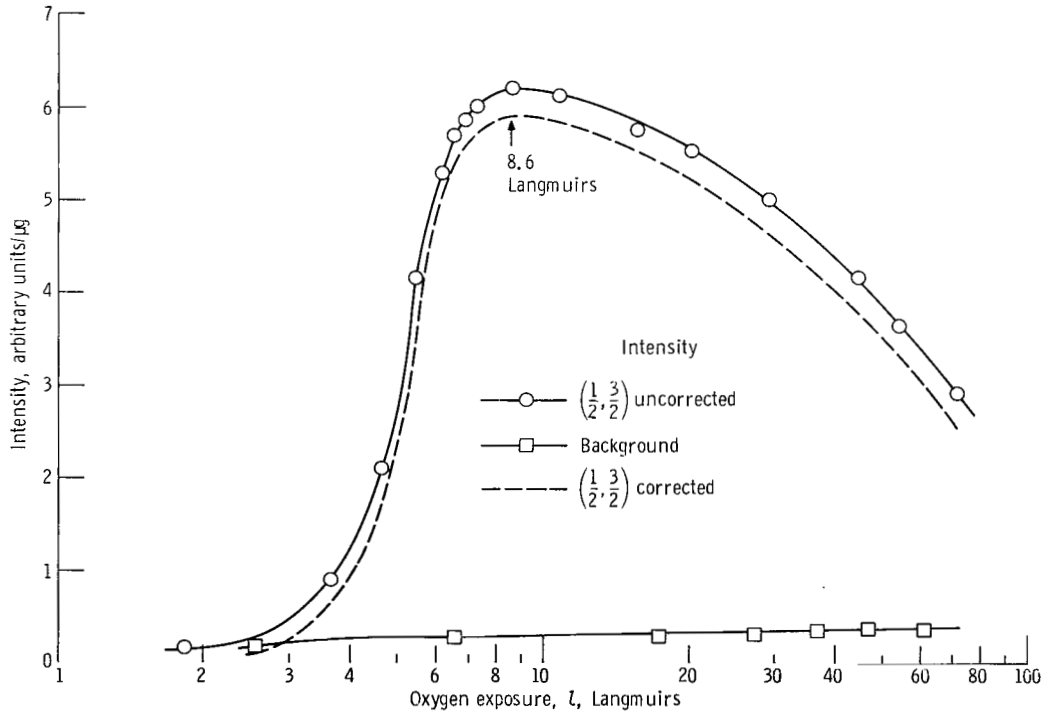

Figure 9. - Intensity of p(2x1) pattern as a function of oxygen exposure.

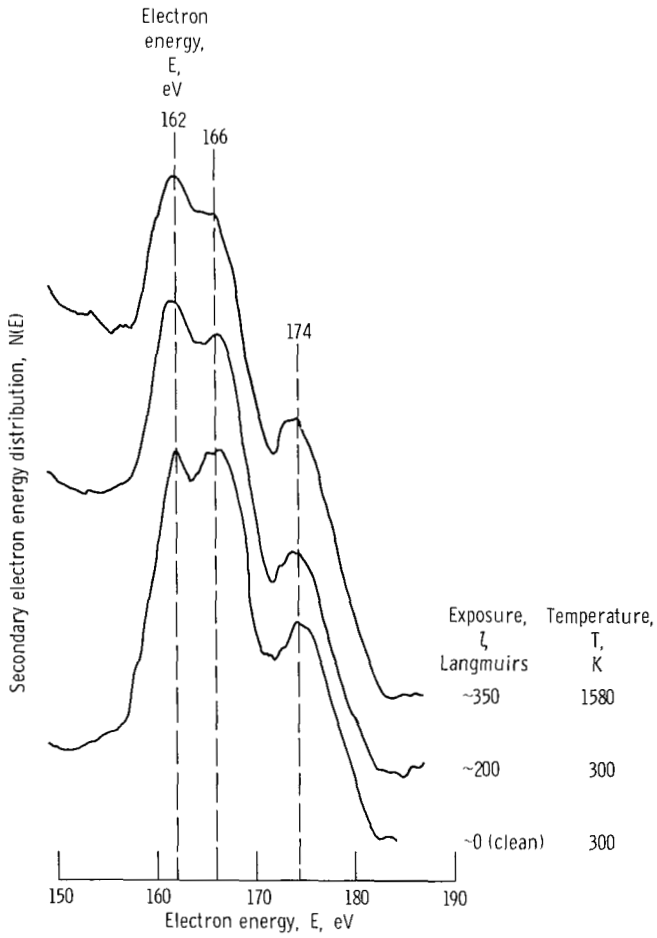

Figure 11. - Tungsten Auger peaks under various surface conditions. Beam energy E_0 = 340 eV.

Figure 10. - LEED pattern at 83 eV after heating W(110) at 1250 K for exposure of 106 Langmuirs.

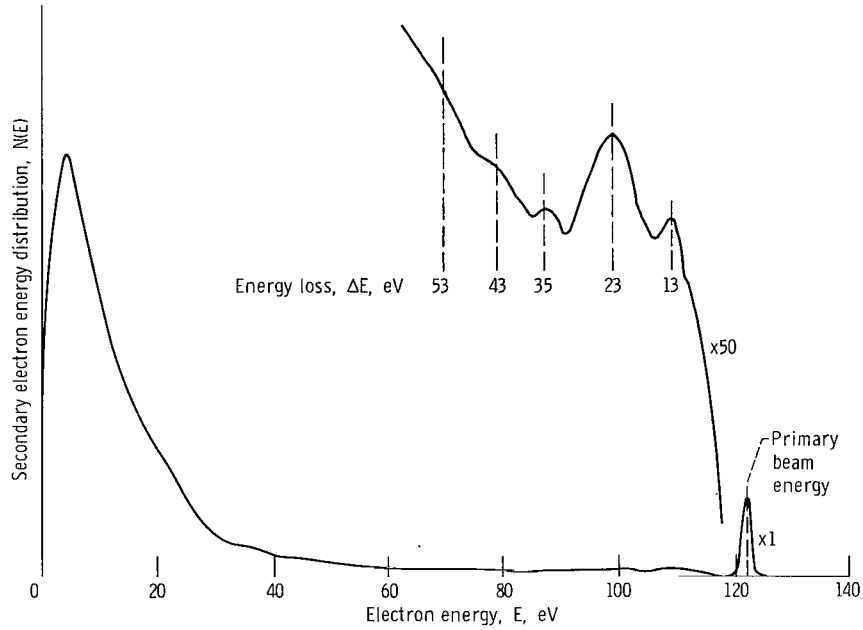

Figure 12. - Secondary electron energy distribution for 122-eV peimary electrons on clean W(110).

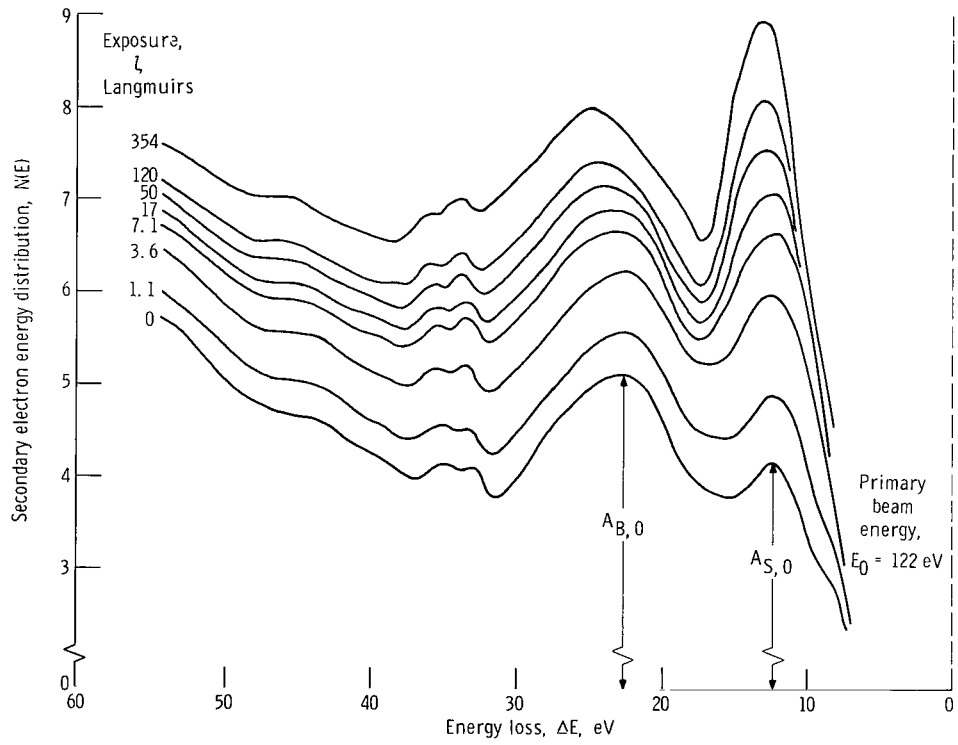

Figure 13. - Dependence of characteristic energy losses on oxygen exposure. Peak-to-peak modulation amplitude 2v = 1/2 volt; total sweep rate R_T = 0.25 volt per second; lock-in amplifier time constant T_{RC} = 1 second.

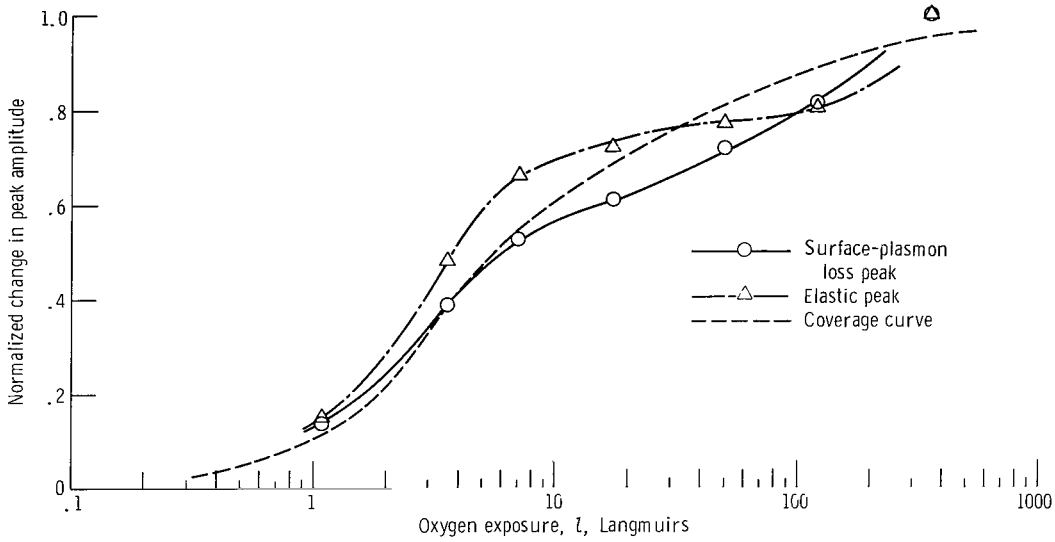

Figure 14. - Normalized change in surface-plasmon and elastic peaks as a function of oxygen exposure.

CS-588-2

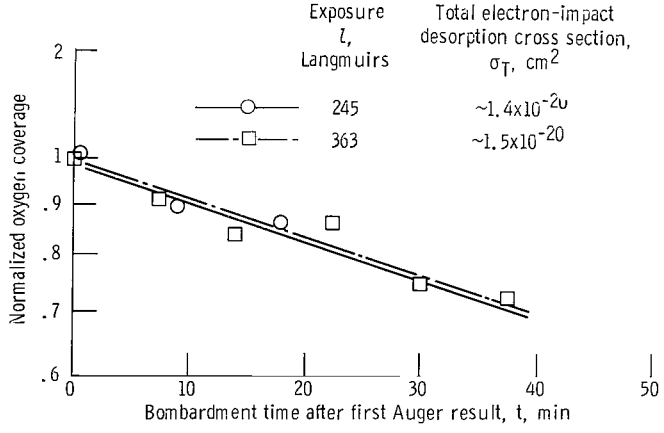

Figure 15. - Oxygen coverage on W(110) as a function of bombardment time. Beam energy, E_0 = 1365 eV.

CS-588-1

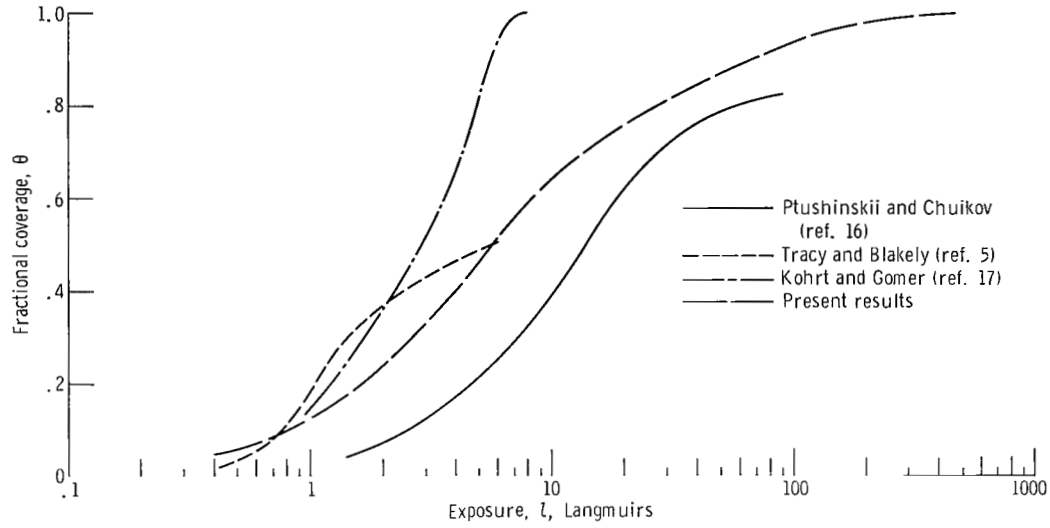

Figure 16. - Comparison of various results for oxygen coverage as a function of oxygen exposure.

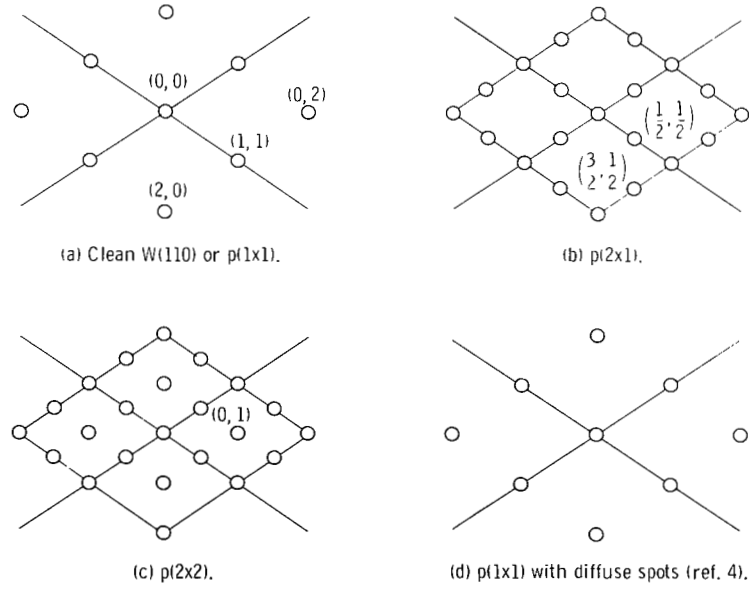

Figure 17. - W(110) LEED patterns at a beam energy of ~120 eV as a function of oxygen coverage.

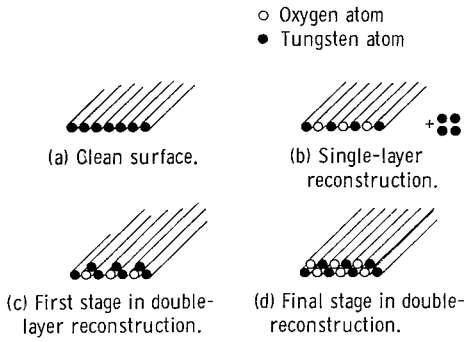

Figure 18. - Schematic of p(2x1) reconstruction models for W(110).

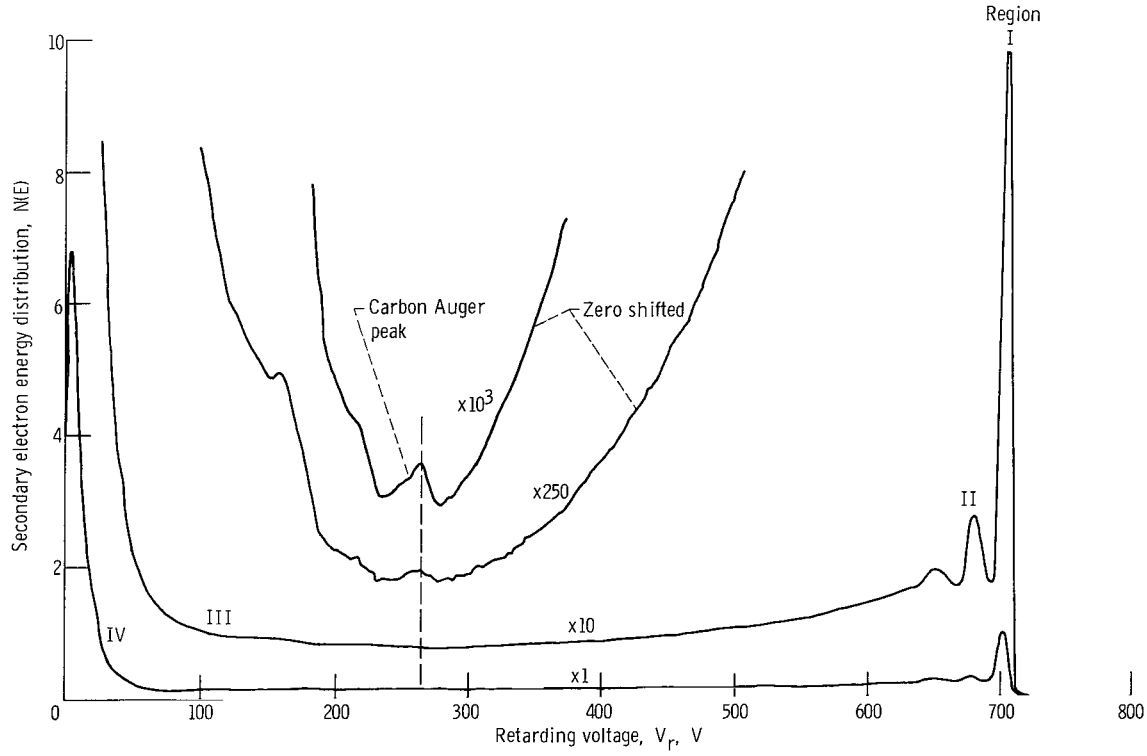

Figure 19. - Secondary electron energy distribution for carbon-contaminated W(110). Primary beam energy E_0 = 698 eV.

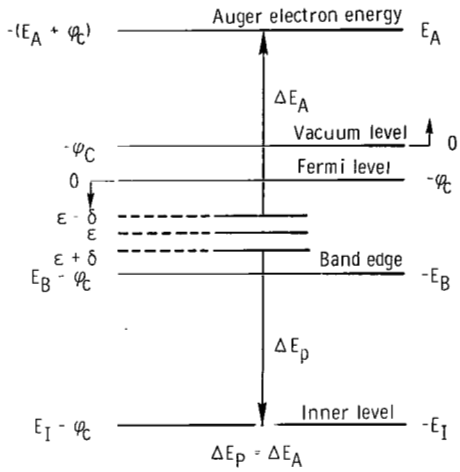

$$E_A = E_I - 2(\varphi_c + \varepsilon)$$

CS-49460

and

$$E_A = E_M + \varphi_G$$

Figure 20. - Auger transition diagram.

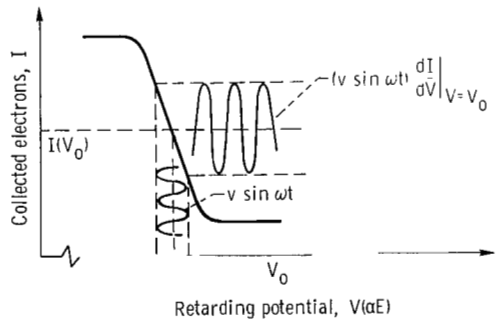

Figure 21. - Retarding-potential modulation technique where

$$I(E) = I(E_0) + \left.\frac{dI}{dE}\right|_{E=E_0} (E - E_0) + \frac{1}{2!} \left.\frac{d^2I}{dE^2}\right|_{E=E_0} (E - E_0)^2 + \frac{1}{3!} \left.\frac{d^3I}{dE^3}\right|_{E=E_0} (E - E_0)^3 + \ldots$$

$$= I(E_0) + N(E_0) \sin \omega t + \frac{\varepsilon^2}{4} \left.\frac{dN}{dE}\right|_{E=E_0} (1 - \cos 2\omega t) + \frac{\varepsilon^3}{24} \left.\frac{d^2N}{dE^2}\right|_{E=E_0} (3 \sin \omega t - \sin 3\omega t) + \ldots$$

CS-49459

using $E - E_0 = \varepsilon \sin \omega t$ and $N(E) = dI/dE$.

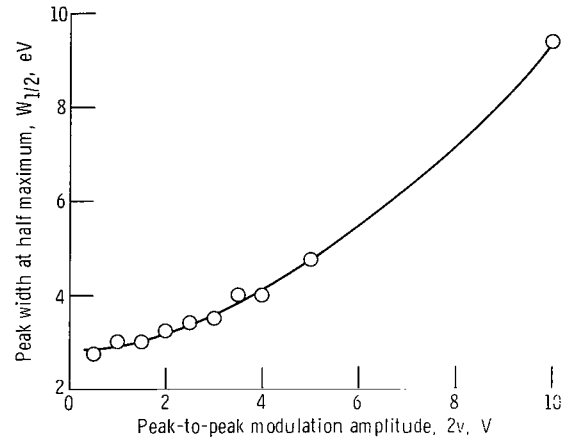

Figure 22. - Variation of width of elastic peak with modulation voltage for 518-eV electrons scattered off oxygen-covered W(110).

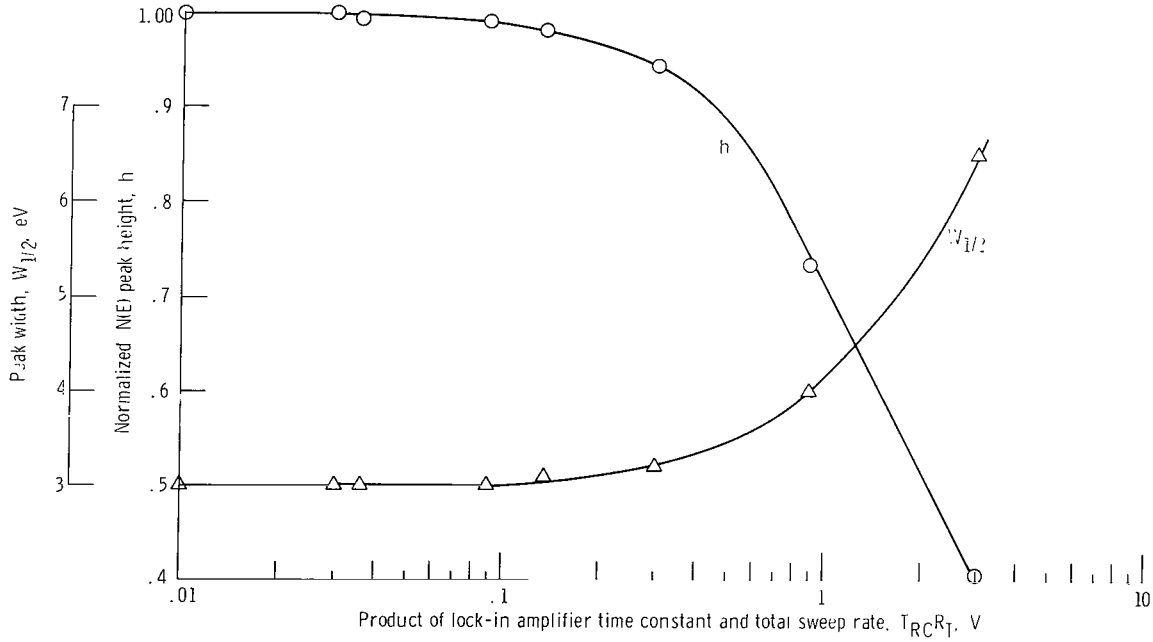

Figure 23 - Relative elastic peak height and width as functions of $T_{RC}R_T$ for 518-eV electrons scattered off oxygen-covered W(110). Peak-to-peak modulation amplitude 2v = 2 volts. (30 msec $\leq T_{RC} \leq$ 10 sec; 0.3 V/sec $\leq R_T \leq$ 3 V/sec).

007 001 C1 U 26 710730 S00903DS
DEPT OF THE AIR FORCE
WEAPONS LABORATORY /WLOL/
ATTN: E LOU BOWMAN, CHIEF TECH LIBRARY
KIRTLANC AFB NM 87117

"The aeronautical and space activities of the United States shall be conducted so as to contribute . . . to the expansion of human knowledge of phenomena in the atmosphere and space. The Administration shall provide for the widest practicable and appropriate dissemination of information concerning its activities and the results thereof."

— NATIONAL AERONAUTICS AND SPACE ACT OF 1958

NASA SCIENTIFIC AND TECHNICAL PUBLICATIONS

TECHNICAL REPORTS: Scientific and technical information considered important, complete, and a lasting contribution to existing knowledge.

TECHNICAL NOTES: Information less broad in scope but nevertheless of importance as a contribution to existing knowledge.

TECHNICAL MEMORANDUMS: Information receiving limited distribution because of preliminary data, security classification, or other reasons.

CONTRACTOR REPORTS: Scientific and technical information generated under a NASA contract or grant and considered an important contribution to existing knowledge.

TECHNICAL TRANSLATIONS: Information published in a foreign language considered to merit NASA distribution in English.

SPECIAL PUBLICATIONS: Information derived from or of value to NASA activities. Publications include conference proceedings, monographs, data compilations, handbooks, sourcebooks, and special bibliographies.

TECHNOLOGY UTILIZATION PUBLICATIONS: Information on technology used by NASA that may be of particular interest in commercial and other non-aerospace applications. Publications include Tech Briefs, Technology Utilization Reports and Technology Surveys.

Details on the availability of these publications may be obtained from:

SCIENTIFIC AND TECHNICAL INFORMATION OFFICE

NATIONAL AERONAUTICS AND SPACE ADMINISTRATION

Washington, D.C. 20546